16th World Conference on Earthquake, 16WCEE 2017

Santiago Chile, January 9th to 13th 2017

Paper N° 4826

Registration Code: S-N1462795827

NONLINEAR MESOSCALE MODELING OF URM STRUCTURES UNDER CYCLIC LOADING

E. Minga [1], L. Macorini [2], B.A. Izzuddin [3]

[1] *PhD student, Department of Civil and Environmental Engineering, Imperial College London, UK, e.minga13@ic.ac.uk*
[2] *Lecturer, Department of Civil and Environmental Engineering, Imperial College London, UK*
[3] *Professor of Computational Structural Mechanics, Department of Civil and Environmental Engineering, Imperial College London, UK*

Abstract

Given the significant seismic vulnerability and complex behaviour of unreinforced masonry (URM) structures, detailed numerical modelling is necessary to provide better understanding and reliable prediction of their response under earthquake loading. However the development of accurate numerical models for URM remains a major challenge, due to the characteristics of the material, most notably the strong influence of the mesostructure and of the properties of the constituents. In previous research, most approaches employ macroscale or 2D mesoscale models, failing to fully represent the material in a generic way. Certain more advanced 3D mesoscale approaches have been developed mostly for monotonic loading conditions and their scale of application is restricted by the increased computational cost. This work proposes a modelling strategy which allows accurate full 3D simulation of URM under cyclic loading conditions with robustness and computational efficiency. A 3D quadratic mesoscale model is employed and a novel cyclic interface constitutive law is presented. The model is incorporated in a hierarchic partitioning framework which significantly reduces the computational cost broadening its applicability.

Keywords: mesoscale model, frictional interface material model, cyclic loading, nonlinear behaviour of URM structures

1. Introduction

Unreinforced masonry (URM) is a material widely used in historical structures and in a number of modern constructions, for example low rise buildings and cladding walls in steel and RC infill frame buildings. Small-scale buildings with principal structural components made of URM are still constructed, especially in zones with limited financial means, many of which exhibit high seismic risk. Thus the accurate FE modelling of the behaviour of URM in the pre- and post-peak regime is a crucial tool for design and assessment purposes. In general, unreinforced masonry presents a complex anisotropic behaviour due to the interaction among the different constitutive components. The mechanical response at structural scale depends on the properties of each constituent and is strongly connected to the mesostructure of the material. As a result, the development of a generic modelling approach describing URM components with arbitrary geometrical and material characteristics remains a major challenge.

Macroelements are often used to account for the influence of URM components in coupled structures or for the modelling of full URM constructions [1-3]. This approach, although practical, is purely phenomenological and overly simplified to provide insight into the various parameters that define the wide response spectrum of masonry. Macroscale constitutive models [4-6] describe masonry as homogeneous material on a structural scale and are often chosen due to their relative simplicity. However, this approach requires a cumbersome parameter identification process which is not always possible, and it may lead to inaccurate failure mode predictions. Mesoscale modelling approaches allow a more realistic representation and response prediction. In this case each constituent is modelled explicitly, hence the identification of the model parameters relies on the identification of the basic material properties of each constituent. Most mesoscale approaches allowing for degradation of strength and stiffness under cyclic loading are developed in 2D, thus restricting the model to in-plane simulations of regular bonding patterns [7-9]. More recently, a few 3D models have been developed considering the possibility of cyclic loading [10,11], with their applications being restricted to single masonry components – e.g. walls, arches – due to the increased computational cost.

In this work an advanced computational strategy is proposed as an efficient tool for the investigation of masonry structures under earthquake loading. A 3D mesoscale description of masonry is employed. Masonry units are modelled with continuum solid elements while mortar and brick-mortar joints are represented with zero-thickness interface elements accounting for both geometric and material nonlinearity, as in previous research investigating URM structures under monotonic loading up to collapse [12,13]. In order to extend the application of the mesoscale model to cyclic loading conditions, a novel cohesive fracture material model for the interface elements has been developed. The model is based on coupling multi-surface plasticity and damage and aims at capturing the main characteristics of the cyclic behaviour of masonry joints - i.e. permanent strains, strength and stiffness degradation and hysteretic behaviour - in a conceptually simple and robust way. The computational cost implicated in the above strategy is significantly reduced with the use of a hierarchic partitioning framework, extending the applicability of the model to the structural scale. Initial results on structural components and numerical-experimental comparisons demonstrate the potential of the strategy for the simulation of in-plane and out-of-plane cyclic behaviour of URM.

2. Partitioned mesoscale modelling of masonry structures

In masonry structures, bricks and blocks generally experience small deformations, while crack paths initiate and develop mainly along the mortar joints. Cracks can also traverse blocks, usually dividing them in two parts through a unique failure surface. The existence of predefined potential failure surfaces renders the use of cohesive interface elements suitable for the simulation of URM.

Based on the above observation, the mesoscale model used here for the simulation of the nonlinear behaviour of URM combines 3D continuum solid elements – for the discretisation of the blocks – with 2D zero-thickness cohesive interface elements – representing the mortar joints combined with the brick mortar interfaces. In addition, the possibility of block failure in tension and shear is included by arranging zero-thickness interface elements in the mid-plane of each block (see Fig.1). The 20-noded solid brick-elements employ a standard linear

elastic material model based on Green's strain. Consequently, the 16-noded interface elements account for both the geometric and material nonlinearity of the model. The geometric nonlinearity is treated with the use of a co-rotational approach, in which the local reference system of the zero-thickness interface element moves together with the mid-plane of the element [12,14]. The nonlinear material behaviour is presented in detail in the following section.

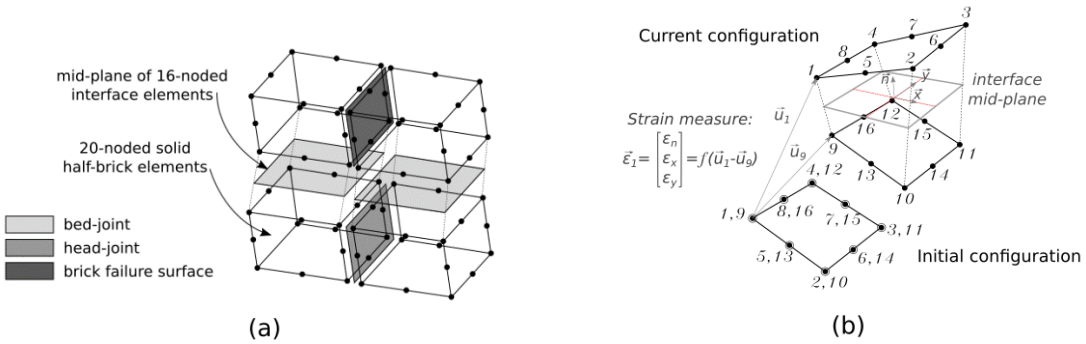

Fig. 1 – (a) Mesoscale modelling of brick masonry; (b) Deformation of 16-noded interface elements

The 3D mesoscale description allows the realistic representation of any bonding pattern, considering both the in-plane and the through-thickness geometry. The only important drawback of the strategy is the increased computational cost, due to the size of the FE model. In order to tackle this issue a domain decomposition framework is employed. The structure is divided in smaller partitions and each of them is analysed in parallel in a different processor, accelerating significantly the procedure. The method employed here [15] uses dual super-elements, consisting of the nodes on the partition boundaries, as "parent structures". The super-elements achieve a two-way communication between the partitions through an interface displacement frame method at the level of the parent structure. They also allow the hierarchic partitioning of the structure, as illustrated in Fig.2, which results in further improvement of the performance.

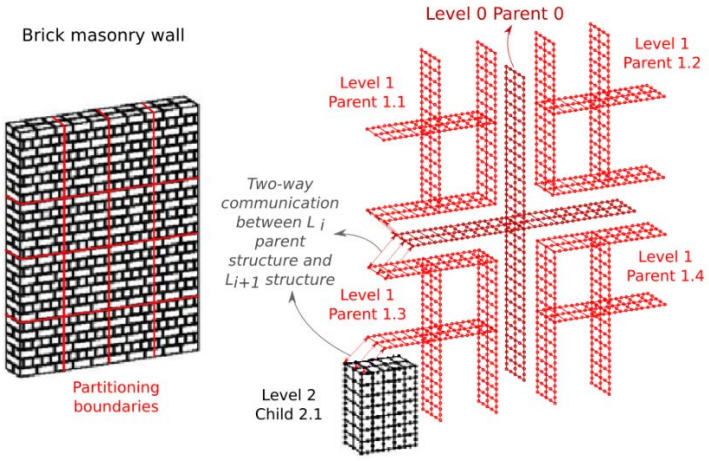

Fig. 2 – Modelling with hierarchic partitioning

3. Interface constitutive model

The material constitutive law defines the relation between the interface tractions **σ** (stress measure) and the interface relative displacements **ε** (strain measure). The aim is to model all the principal characteristics of the constitutive behaviour of a mortar joint or a dry frictional interface – when mortar is absent – with the simplest

possible formulation in order to increase the efficiency and ensure numerical robustness. The most important of these characteristics are i) the softening behaviour in tension and shear, ii) the stiffness degradation depending on the level of damage, iii) the recovering of normal stiffness in compression and iv) the permanent (plastic) strains at zero stresses when the interface is damaged. Additionally, as the nonlinearity of the model is concentrated in the interface elements, the effect of masonry crushing in compression is taken into account in a phenomenological way, through negative plastic normal strain in the interfaces of the crushed area.

The stress and strain measures consist of three components corresponding to the normal and the two tangential directions of the interface mid-plane, see Fig. 1 (b). The basis of the chosen formulation is the coupling of plasticity and damage and the constitutive relation has the following form:

$$\boldsymbol{\sigma} = (\boldsymbol{I} - \boldsymbol{D})\,\tilde{\boldsymbol{\sigma}} = (\boldsymbol{I} - \boldsymbol{D})\,\boldsymbol{K_0}\,(\boldsymbol{\varepsilon} - \boldsymbol{\varepsilon^P}) \tag{1}$$

where $\boldsymbol{\sigma} = [\sigma_n \;\; \tau_x \;\; \tau_y]^T$ is the vector of nominal stresses, $\tilde{\boldsymbol{\sigma}} = [\tilde{\sigma}_n \;\; \tilde{\tau}_x \;\; \tilde{\tau}_y]^T$ the vector of the effective stresses, $\boldsymbol{I}$ the identity matrix, $\boldsymbol{D}$ the diagonal damage tensor, $\boldsymbol{K_0}$ the diagonal elastic stiffness matrix, $\boldsymbol{\varepsilon} = [\varepsilon_n \;\; \varepsilon_x \;\; \varepsilon_y]^T$ the strain vector and $\boldsymbol{\varepsilon^P} = [\varepsilon_n^p \;\; \varepsilon_x^p \;\; \varepsilon_y^p]^T$ the corresponding plastic strain vector. As derived by Eq. (1), the plastic strains are coupled to the effective stresses. The damage tensor is calculated after the solution of the plastic problem as a function of the plastic work produced, and the nominal stresses are obtained by applying the damage to the effective stresses. By algorithmically decoupling the implicit solution of the plastic problem and the damage evolution – following the idea presented in [16] – increased efficiency and robustness is achieved.

3.1 Multi-surface plasticity

For the effective stress-based plasticity problem, a multi-surface limit domain is used, as shown in Fig. 3. The domain is defined by the tensile yield surface F_1, the shear yield surface F_2 and the compressive cap surface F_3. Surface F_2 is the typical frictional yield surface, which well represents the shear behaviour of joints according to experimental data [17]. It is defined by the cohesion c and the friction angle φ. Surfaces F_1 and F_3 are simplified linear approximations of the caps in tension and compression, defined by the limit strength of the joint in direct tension f_t and the limit strength of masonry in direct compression f_c.

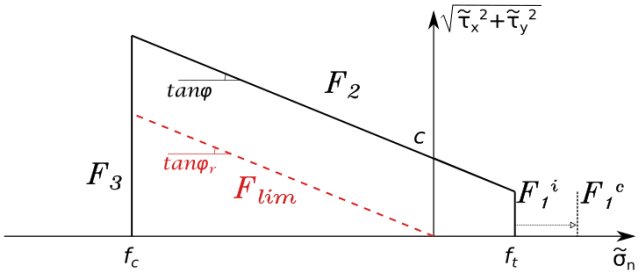

Fig. 3 – Limit domain of effective stresses

The possibility of hardening is introduced in surface F_1 in order to control the amount of plastic strains – i.e. control the level of stiffness degradation. The complete multi-surface plasticity problem is described by the following set of equations:

$$\tilde{\boldsymbol{\sigma}} = \boldsymbol{K_0}(\boldsymbol{\varepsilon} - \boldsymbol{\varepsilon^{p,1}} - \boldsymbol{\varepsilon^{p,2}} - \boldsymbol{\varepsilon^{p,3}}) \tag{2}$$

$$q = -H\kappa \tag{3}$$

$$F_1 = \tilde{\sigma}_n - (f_t + q) \leq 0 \tag{4}$$

$$F_2 = \sqrt{\tilde{\tau}_x^2 + \tilde{\tau}_y^2} + \tilde{\sigma} \tan\varphi - c \leq 0 \tag{5}$$

$$F_3 = -\tilde{\sigma}_n + f_c \leq 0 \tag{6}$$

$$\dot{\boldsymbol{\varepsilon}}^{\boldsymbol{p,1}} = \dot{\lambda}_1 \frac{\partial F_1}{\partial \tilde{\boldsymbol{\sigma}}}, \quad \dot{\boldsymbol{\varepsilon}}^{\boldsymbol{p,2}} = \dot{\lambda}_2 \frac{\partial G_2}{\partial \tilde{\boldsymbol{\sigma}}}, \quad \dot{\boldsymbol{\varepsilon}}^{\boldsymbol{p,3}} = \dot{\lambda}_3 \frac{\partial F_3}{\partial \tilde{\boldsymbol{\sigma}}} \tag{7-9}$$

$$\dot{\kappa} = \dot{\lambda}_1 \frac{\partial F_1}{\partial q} = -\dot{\lambda}_1 \tag{10}$$

Non-associated plasticity is used for the plastic strain $\boldsymbol{\varepsilon}^{\boldsymbol{p,2}}$ to control the level of dilatancy. The plastic potential G_2 has the same form as F_2 but a different friction angle $tan\varphi_g$, generally smaller or tending to zero according to experimental evidence on the dilatancy of masonry joints under shear [17].

The hardening modulus H controls the level of stiffness degradation in the normal direction, according to the logic demonstrated in Fig. 4. In this figure we denote as ε_f the normal strain for which the damage in the normal direction becomes equal to 1.

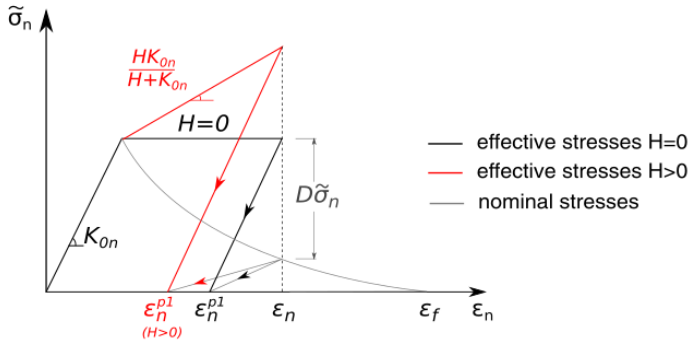

Fig. 4 – Control of stiffness degradation in the normal direction through hardening

The value of H depends on the material parameter μ which is equal to the ratio of the plastic (permanent) normal strain $\varepsilon_n^{p,1}$ if the unloading begins from the point of full damage ($\varepsilon_n = \varepsilon_f$) divided by ε_f. H is given by the following equation:

$$H = \frac{K_{0,n}\varepsilon_f(1-\mu) - f_t}{\varepsilon_f\,\mu} \tag{11}$$

Regarding the tangential direction, there is no hardening associated with F_2, hence the amount of stiffness degradation is simply coupled to the level of damage and is bound by the permanent strains produced in the elastic-perfectly-plastic evolution of the effective stresses. This simplification is justified by the experimental data on cyclic shear behaviour of masonry joints which reveal that stiffness degradation is not a prevailing factor in shear and that it is limited to a low level [17-18].

3.2 Damage

The damage of the interface is defined by three scalar damage variables – D_t for the normal direction in tension, D_c for the normal direction in compression and D_s for the two tangential directions – which compose the diagonal damage tensor $\boldsymbol{D} = \boldsymbol{diag}\{D_n, D_s, D_s\}$, where $D_n = D_t$ if $\tilde{\sigma} \geq 0$ and $D_n = D_c$ if $\tilde{\sigma} < 0$. The decomposition of D_n results in the recovering of the normal elastic stiffness in compression.

The behaviour of the interface is defined by three main deformation modes – tension, shear and compression – each one corresponding to one of the yield surfaces F_1, F_2 and F_3 respectively. $\boldsymbol{D}$ is a function of the ratio of the plastic work $W_{cr,i}$ produced in the interface for each mode i divided by the fracture energy corresponding to the same mode $G_{cr,i}$.

$$0 \leq \frac{W_{cr,i}}{G_{cr,i}} = \frac{\tilde{\boldsymbol{\sigma}} \cdot \boldsymbol{\varepsilon}^{\boldsymbol{p},\boldsymbol{i}}}{G_{cr,i}} \leq 1 \tag{12}$$

Physically, the damage of the interface in tension or shear influences the behaviour in both the tensile and shear mode, but it has no significant influence in the crushing mode. On the contrary, the behaviour in shear is influenced by the crushing in compression. Based on the above assumptions, the damage variables depend on the plastic work of each mode as follows:

$$D_t = d_t\left(\frac{W_{cr,1}}{G_{cr,1}}, a_t \frac{W_{cr,2}}{G_{cr,2}}\right) \tag{13}$$

$$D_c = d_c\left(\frac{W_{cr,3}}{G_{cr,3}}\right) \tag{14}$$

$$D_s = d_s\left(\frac{W_{cr,1}}{G_{cr,1}}, \frac{W_{cr,2}}{G_{cr,2}}, a_s \frac{W_{cr,3}}{G_{cr,3}}\right) \tag{15}$$

The form of the functions d_t, d_c and d_s defines the shape of the softening branch of the **σ-ε** relation. In this formulation, a second order polynomial function with respect to the ratio $W_{cr,i}/G_{cr,i}$ is used for d_t and d_s, while a sinusoidal function is employed for d_c.

3.3 Residual shear stresses

A frictional interface completely damaged in shear holds a residual shear stress under compression which depends on the level of the normal compressive stress – as described by the Coulomb criterion. A good approximation of this shear stress residual is given by the surface F_{lim} in Fig. 3.

$$F_{lim} = \sqrt{\tau_x^2 + \tau_y^2} + \sigma \tan \varphi_r \tag{16}$$

In order to obtain this residual in the nominal shear stresses, the fully damaged state ($D_s = 1$) in the compressive region corresponds to a nominal shear stress on F_{lim} instead of zero, see Fig. 5. The angle φ_r represents the residual friction angle of the damaged joint which is usually considered equal to the initial friction angle φ. However, it can assume a lower value if deemed appropriate, for example in the case of dry joints [18].

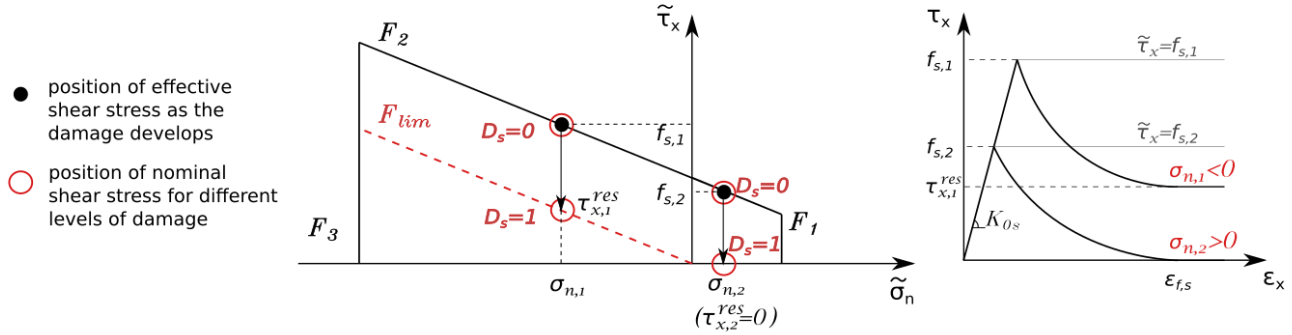

Figure 5 – Shear stress residual based on Coulomb friction

4. Numerical analyses of URM components

In this section the modelling approach introduced above is used for the analysis of URM structural elements under different types of loading. A wide range of URM behavioural characteristics is explored and the accuracy and potential of the numerical model is shown through a series of numerical-experimental comparisons. All the analyses were performed using ADAPTIC [19].

4.1 In-plane cyclic behaviour of URM pier wall

The study of the in-plane cyclic response is based on the experiments performed at the Joint Research Centre of the European community in Ispra, Italy [20]. In order to examine the variation in the failure modes and the cyclic in-plane behaviour characteristics of walls of different aspect ratios (height/width), quasi-static cyclic tests were performed for two walls with aspect ratio 1.35 and 2.00.

Table 1 – Walls in-plane: material parameters of mortar joints in mesoscale model

K_n (N/mm^3)	K_t (N/mm^3)	f_t (N/mm^2)	c (N/mm^2)	tanφ	tanφ$_g$	f_c (N/mm^2)	G_{f1} (N/mm)	G_{f2} (N/mm)	G_{f3} (N/mm)
48.00	21.00	0.04	0.23	0.58	0.00	6.2	0.05	0.10	1.00

The dimensions of the walls are 1000×1350 mm^2 and 1000×2000 mm^2 respectively with 250 mm thickness. The walls were built with brick-block units of 250×120×55 mm^3 arranged in a two-wythe thick English bond pattern. The thickness of the joints is 10 mm. The bottom of the walls is connected to the fully fixed "ground" through a bed joint. A steel beam which was prevented from rotating was placed on top of each wall, transferring a uniform compressive pressure of 0.6 MPa and providing a slab support. Horizontal in-plane displacement cycles of increasing magnitude were then imposed to the beam.

The boundary and loading conditions were modelled in detail, as described above. The material parameters of the mesoscale model were chosen based on the results reported in [21] from experiments performed on the materials used for the construction of the walls. The values of the parameters for the mortar joints are summarised in Table 1.

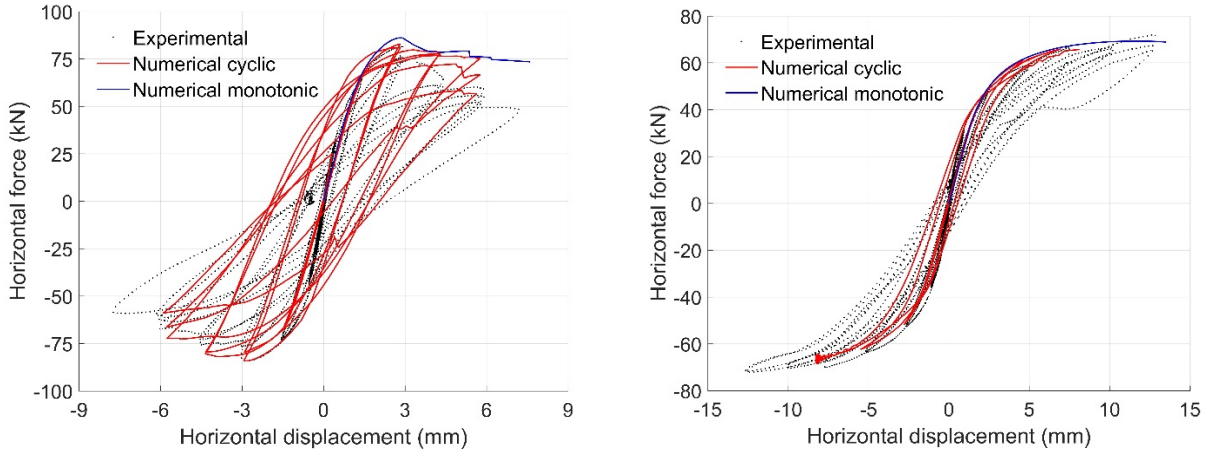

Figure 6 – Numerical-experimental comparison of short wall (left) and tall wall (right) under in-plane cyclic loading

Fig.6 shows experimental and numerical comparisons of the horizontal force-displacement diagrams for the two walls. The displacement refers to the horizontal displacement imposed to the top beam. Fig.7 presents the failure modes observed in the two walls under monotonic loading (for clarity) in stages of the numerical analysis with advanced damage.

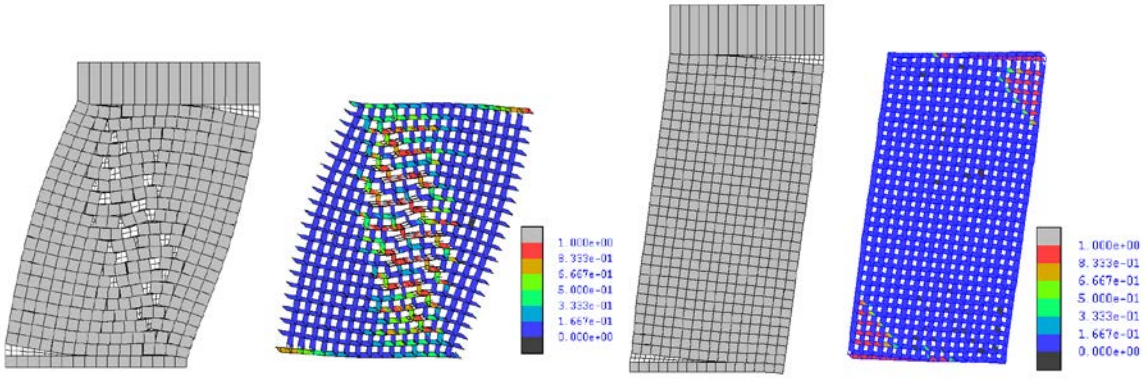

Figure 7 – Deformed shapes and damage developed at the interfaces in the short and the tall wall for monotonic loading

The predicted damage and failure modes for the two walls compare well against the distinct cracking patterns observed during the experiments [20]. The short wall presents diagonal cracking along its height, horizontal cracks and crushing close to the corners. Meanwhile, the damage of the tall wall is flexural and is mainly concentrated at the top and bottom bed joints, which are fully damaged in the tensile direction; the cyclic response of the tall wall is a type of rocking behaviour. Regarding the force-displacement diagrams, the load at the onset of damage and the peak load are reproduced with accuracy in both cases. The hardening envelope of the cyclic response of the tall wall is accurately captured. The softening envelope of the short wall is reproduced well in the negative quadrant, but is not fully captured in the positive quadrant in the first displacement cycles. Furthermore, progressively increasing stiffness degradation is observed at structural level for the short wall. The amount of degradation is less than that obtained experimentally in the first displacement cycles, but the difference is significantly reduced as the damage progresses. Both the strength and stiffness degradation are related to the fracture energy parameters, which might not be well identified. While a parametric study is out of the scope of this paper, it will be a topic of further investigation.

4.2 Out-of-plane flexure and rocking of URM wall

A study of certain characteristics of the static and dynamic out-of-plane behaviour of simply supported URM walls has been investigated by Griffith et al. [22] and presented in more detail in [23]. Walls with and without pre-compression – representing correspondingly the load bearing and non-load bearing type – were tested under static monotonic loading and dynamic excitations in the out-of-plane direction. A distinction was made between "uncracked" and "cracked" walls, the later having sustained damage in previous rounds of the experimental testing. A database with the distinct out-of-plane response in each of the above cases was collected.

Table 2 – Walls in out-of-plane flexure and rocking: material parameters of mortar joints in mesoscale model

Condition	K_n (N/mm^3)	K_t (N/mm^3)	f_t (N/mm^2)	c (N/mm^2)	tanφ	tanφ$_g$	f_c (N/mm^2)	G_{f1} (N/mm)	G_{f2} (N/mm)	G_{f3} (N/mm)
new	250.00	105.00	0.163	0.24	0.75	0.00	13.40	0.05	0.10	1.00
damaged	10.00	5.00	0.01	0.01	0.75	0.00	13.40	0.01	0.01	1.00

We have investigated the capacity of the presented model to reproduce certain key characteristics of the out-of-plane monotonic and rocking behaviour observed experimentally. The wall of 110 mm thickness, with slenderness ratio (height/thickness) of 13.6 has been modelled. The height of the specimens is 1500 mm and the width 950mm, with brick units of dimensions 230×110×76 mm^3. The material properties provided in [23] are limited and refer to masonry at a macroscopic level. Therefore, the parameters used for the mesoscale model were derived based on average values of constituents' properties in newly constructed masonry and on previously suggested relations between the macroscopic and the microscopic properties of masonry [24]. The tensile strength of the mortar joints f_t, which is the key parameter for the out-of-plane resistance of the walls, has been calculated by the flexural strength of masonry through the simple relation $f_t=1/3 \cdot f_{mt}$, following the suggestion of Milani [24]. For the analyses of the cracked walls, the bed joints at the bottom and at mid-height of the wall have been considered severely damaged. This is achieved by applying low tensile yield stress, low fracture energy and low elastic stiffness parameters in the material model of the corresponding interface elements. A summary of the parameters employed is provided in Table 2.

The bottom of the walls is supported in the direction of the loading at the level of the bottom bed joint. The top boundary conditions of the non-load bearing wall consist of simple translation supports in the direction of the loading. In the load bearing walls, in addition to the same simple support, a stiff beam has been added on top. The beam is in unilateral contact with the wall, transferring the vertical loads and providing a slab support. In the experimental setting the compressive load is applied through springs. As a result, the level of the load increases as the wall deforms [22]. This condition was modelled by adding spring elements in the vertical direction on top of the slab.

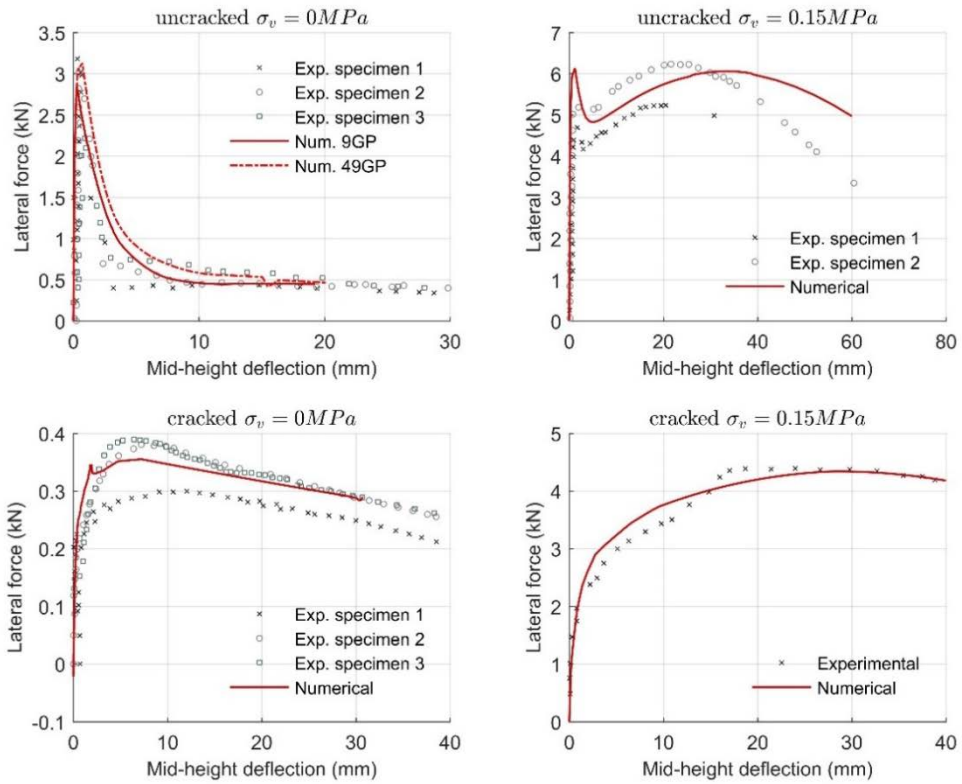

Figure 8 – Walls in out-of plane flexure: experimental numerical comparison of pushover curves

Initially, the static pushover test was reproduced. Displacements were imposed at the mid-height of the wall to obtain the complete pre- and post-peak force-displacement curve. The results, shown in Fig.8, demonstrate the potential of the mesoscale FE model to accurately predict the pushover envelopes given the

different boundary and material conditions. Accurately reproducing both the peak lateral loads – i.e. ultimate strength – and the corresponding displacements, the model gives a complete picture of the flexure response overcoming the limitations of the classical simplified theories of linear elastic and rigid body analysis, as highlighted in [22].

Subsequently, the real earthquake tests that were performed in the shaking table were simulated. The top and bottom of the walls are subjected simultaneously to the same accelerations, which correspond to Ground Motion Records (GMR) of two earthquakes – the 1940 El Centro and the 1994 Pacoima Dam earthquake – multiplied by the factors 0.66, 0.80 and 1.00. The displacement records produced in the shaking table during the experiment, as reported in [22], are relatively close to the displacement GMR of the earthquakes but do not coincide. For the dynamic analyses, an additional modelling consideration – the influence of which is highlighted in [22] – is the damping. The model has an "internal" source of stiffness-dependent damping in the joints, due to the nonlinear material model. Additionally, the mass-dependent part of the Rayleigh damping model is considered at structural level. Based on the comments in [22] and [25], damping levels of 3% and 5% are tested.

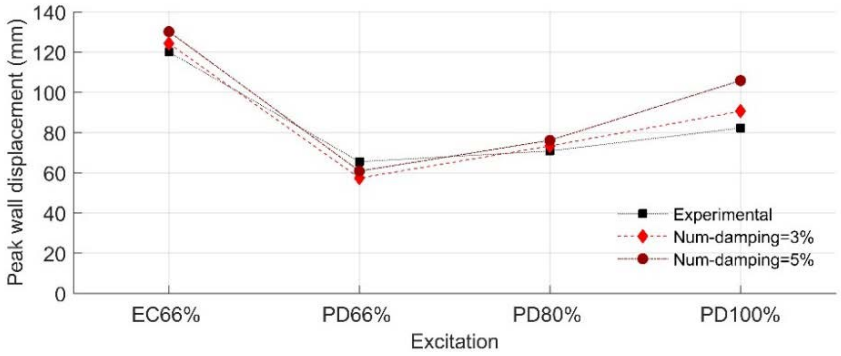

Figure 9 – Rocking out-of-plane: experimental-numerical comparison of PWD for different excitations (EC=El Centro, PD=Pacoima Dam)

Fig.9 presents a comparison of the peak wall displacements (PWD) – i.e. the out-of-plane drift at the mid-height of the wall – obtained experimentally and numerically for each level of excitation. It is reported that the walls collapse in the cases of 80% and 100% El Centro excitation. Collapse was also obtained in the corresponding numerical simulations. It can therefore be concluded that the numerical predictions of the PWD and the final capacity of the walls in real earthquake scenarios – which is dictated by the displacement demand as suggested in [22] – compare well to the experimental observations. Based on this study, a constant damping parameter of ζ=0.03 is recommended for the numerical simulations.

4.3 Two-way bending of URM walls

In real URM structures the boundary conditions around a pier loaded out-of-plane during an earthquake are often more complicated than the ones considered in the example above. Commonly, the sides of a wall panel are connected with lateral URM walls. This two-way bending configuration has been experimentally tested by Griffith et al. [26]. A numerical simulation has been performed in order to examine the potential of the presented modelling approach for the simulation of larger structural elements, with boundary conditions and interactions that are difficult to take into account with more simplified models.

The specimen modelled (specimen 2) consists of a main wall of 4000×2500 mm^2 without openings and 480 mm long return walls on both sides. They are built with clay brick units of 230×110×76 mm^3. The material properties are similar to the ones in the previous section – see Table 2-new – except for the elastic stiffness parameters of the mortar joints. In order to obtain the elastic modulus of masonry reported in [26], the above parameters have the following values: K_n=80N/mm^3 and K_t=36 N/mm^3. The main wall is simply supported along the top and the bottom edge in the direction of the loading. Additionally, restraints are imposed to the

moments and displacements along the vertical edges of the return walls. In the static round of testing, modelled here, uniform pressure is applied at the external face of the main wall, until the ultimate load is exceeded.

Fig.10 shows the experimental-numerical comparison of the pressure-displacement curves and the damage developed in the interfaces of the wall specimen. The ultimate loading obtained numerically is in good agreement with the experimental results, but the corresponding displacement is significantly lower. This is potentially related to an inaccurate estimation of the elastic parameters of the model constituents and/or the values of the fracture energy, properties which are not provided in [26]. The identification of those properties and the analysis of their influence in the out-of-plane behaviour of URM walls will be a topic of further studies.

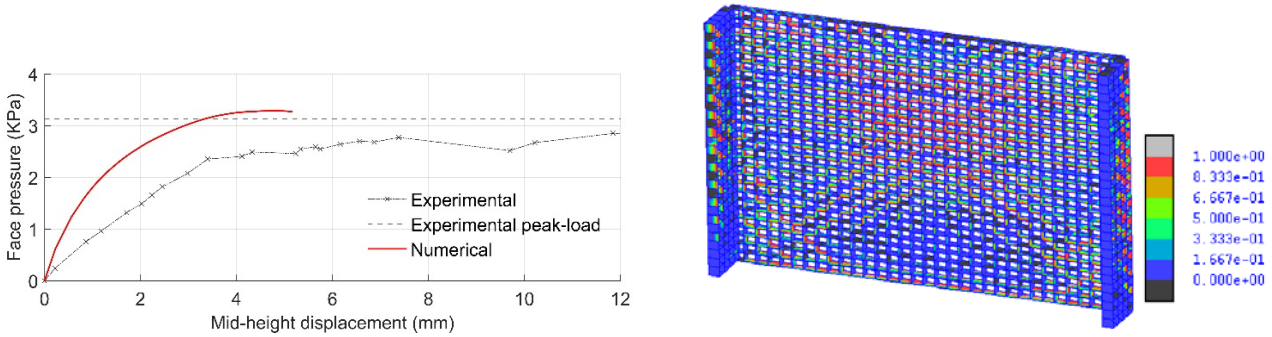

Figure 10 – URM in two-way bending: experimental –numerical comparison of pressure-displacement curve (left) and damage developed in the interface elements at the end of the analysis (right)

Regarding the cracking pattern developed in the model, it consists of diagonal cracking in the central area and around the corners of the main wall, cracking at the bottom bed joint and along some bed joints at mid-height of the main wall and vertical cracking in the return walls close to the connection with the main wall. This pattern is in close agreement with the experimental observations.

5. Conclusion

A detailed FE modelling strategy has been proposed for the simulation of the nonlinear behaviour of URM structures under cyclic loading conditions. A mesoscale approach has been used in which the nonlinearity is concentrated in the mortar joints and the potential failure surfaces of the bricks. The constitutive behaviour of the interfaces is modelled with a novel material model which reproduces the key defining characteristics of the physical behaviour in a simple and robust way, based on the idea of decoupling of plasticity and damage, as proposed by Grassl et al. [16]. The use of a hierarchic partitioning framework has largely increased the efficiency of the strategy and reduced the computational cost. Experimental-numerical comparisons have demonstrated the potential of this approach for the simulation of URM under quasi-static and dynamic loading conditions. The few limitations that have been observed will be further investigated, as the conceptual simplicity of the approach allows further localised enhancements without compromising its robustness. It can be safely concluded that the proposed strategy can be a useful tool for the investigation of the behaviour of URM structures under earthquake loading.

6. References

[1] Magenes, G, Fontana AD (1998): Simplified non-linear seismic analysis of masonry buildings. *Proc. Br. Masonry Society No. 8*, 190-195.

[2] Lagomarsino S, Penna A, Galasco A, Cattari S (2013): TREMURI program: an equivalent frame model for the nonlinear seismic analysis of masonry buildings. *Engineering Structures*, **56**, 1787-1799.

[3] Caliò I, Marletta M, Pantò B (2012): A new discrete element model for the evaluation of the seismic behaviour of unreinforced masonry buildings. *Engineering Structures*, **40**, 327-338.

[4] Lourenço PB, Rots JG, Blaauwendraad J (1998). Continuum model for masonry: parameter estimation and validation. *Journal of Structural Engineering*, **124**(6), 642-652.

[5] Calderini C, Lagomarsino S (2008): Continuum model for in-plane anisotropic inelastic behavior of masonry. *Journal of structural engineering*, **134**(2), 209-220.

[6] Pelà L, Cervera M, Roca P (2013): An orthotropic damage model for the analysis of masonry structures. *Construction and Building Materials*, **41**, 957-967.

[7] Gambarotta L, Lagomarsino S (1997): Damage models for the seismic response of brick masonry shear walls. Part I: the mortar joint model and its applications. *Earthquake engineering & structural dynamics*, **26**(4), 423-439.

[8] Oliveira DV, Lourenço PB (2004): Implementation and validation of a constitutive model for the cyclic behaviour of interface elements. *Computers & structures*, **82**(17), 1451-1461.

[9] Sacco E, Lebon F (2012): A damage–friction interface model derived from micromechanical approach. *International Journal of Solids and Structures*, **49**(26), 3666-3680.

[10] Spada A, Giambanco G, Rizzo P (2009): Damage and plasticity at the interfaces in composite materials and structures. *Computer Methods in Applied Mechanics and Engineering*, **198**(49), 3884-3901.

[11] Aref AJ, Dolatshahi KM (2013): A three-dimensional cyclic meso-scale numerical procedure for simulation of unreinforced masonry structures. *Computers & Structures*, **120**, 9-23.

[12] Macorini L, Izzuddin BA (2011): A non-linear interface element for 3D mesoscale analysis of brick-masonry structures. *International Journal for numerical methods in Engineering*, **85**(12), 1584-1608.

[13] Macorini L, Izzuddin BA (2013). Nonlinear analysis of masonry structures using mesoscale partitioned modelling. *Advances in Engineering Software*, **60**, 58-69.

[14] Izzuddin BA (2005): An enhanced co-rotational approach for large displacement analysis of plates. *International Journal for Numerical Methods in Engineering*, **64**(10), 1350-1374.

[15] Jokhio GA, Izzuddin BA (2015): A dual super-element domain decomposition approach for parallel nonlinear finite element analysis. *International Journal for Computational Methods in Engineering Science and Mechanics*, **16**(3), 188-212.

[16] Grassl P, Rempling R (2008): A damage-plasticity interface approach to the meso-scale modelling of concrete subjected to cyclic compressive loading. *Engineering Fracture Mechanics*, **75**(16), 4804-4818.

[17] Atkinson RH, Amadei BP, Saeb S, Sture S (1989): Response of masonry bed joints in direct shear. *Journal of Structural Engineering*, **115**(9), 2276-2296.

[18] Lourenço, P. B., & Ramos, L. I. S. F. (2004). Characterization of cyclic behavior of dry masonry joints. *Journal of Structural Engineering*, **130**(5), 779-786.

[19] Izzuddin BA (1991): Nonlinear Dynamic Analysis of Framed Structures. *PhD thesis*, Imperial College, University of London, UK.

[20] Anthoine A, Magenes G, Magonette G (1994): Shear compression testing and analysis of brick masonry walls. *Proc. 10th European Conference on Earthquake Engineering*, Vienna, 1657-1662.

[21] Binda L, Tiraboschi C, Mirabella Roberti G, Baronio G, Cardani G (1996): Measuring masonry material properties: detailed results from an extensive experimental research, *Report 5, Politecnico di Milano.*

[22] Griffith MC, Lam NT, Wilson JL, Doherty KT (2004): Experimental investigation of unreinforced brick masonry walls in flexure. *Journal of Structural Engineering*, **130**(3), 423-432.

[23] Doherty KT (2000): An investigation of the weak links in the seismic load path of unreinforced masonry buildings, *PhD thesis*, University of Adelaide, Australia.

[24] Milani G (2008): 3D upper bound limit analysis of multi-leaf masonry walls. *International Journal of Mechanical Sciences*, **50**(4), 817-836.

[25] Lam NT, Griffith M, Wilson J, Doherty KT (2003): Time–history analysis of URM walls in out-of-plane flexure. *Engineering structures*, **25**(6), 743-754.

[26] Griffith MC, Vaculik J, Lam NT, Wilson J, Lumantarna E (2007): Cyclic testing of unreinforced masonry walls in two-way bending. *Earthquake Engineering & Structural Dynamics*, **36**(6), 801-821.